Optical properties of randomly distributed particles

Ansgar Liebsch
Institut für Festkörperforschung, Kernforschungsanlage Jülich, D-5170 Jülich, West Germany and Instituto de Física, Universidad Autónoma de San Luis Potosí, San Luis Potosí, Mexico

Pedro Villaseñor González
Instituto de Física, Universidad Autónoma de San Luis Potosí, San Luis Potosí, Mexico

(Received 17 October 1983)

The optical properties of inhomogeneous media consisting of small metal particles in a dielectric host (cermet topology) are studied using the coherent-potential approximation in conjunction with a lattice-gas model. The theory includes the dipole fields of the randomly distributed particles and constitutes a self-consistent generalization of the Maxwell-Garnett model. It is shown that the disorder leads to a sizable red shift and broadening of absorption peaks. These effects are largest near filling fractions of about 10—20 % in contrast to multipole-induced changes, which become important at higher particle concentrations. The composite dielectric function is shown to satisfy the rigorous bounds which hold for any two-component system. The disorder treatment is extended to multicomponent composites in order to illustrate the effect of nonuniform particle sizes. In the case of two-dimensional inhomogeneous systems, the disorder is shown to have a qualitatively different influence on the shift and broadening of the parallel and perpendicular collective modes. Several applications of the theory to real systems are given and compared with experimental absorption spectra.

I. INTRODUCTION

The remarkable range of electromagnetic properties found in inhomogeneous systems has attracted attention for a long time.[1] In recent years this class of materials has been widely studied because of the potential usefulness as efficient photothermal solar energy converters.[2] In practice, the spectral selectivity that is required for good absorber surfaces (high absorption in the visible and the ultraviolet and low emission at thermal wavelengths to reduce losses due to reradiation) can presumably only be achieved by combining a variety of mechanisms such as surface roughness, interference, intrinsic properties, inhomogeneity, etc.[3] In this regard, composite systems consisting of small metallic particles (diameter ~ 100 Å) dispersed in a dielectric host material are of particular importance for solar-energy conversion since they tend to exhibit large absorption cross sections at visible frequencies.[2]

Recently, a new theoretical method[4,5] has been developed which allows an approximate description of the influence of particle interactions on absorption spectra of composites. The metallic particles are assumed to be completely surrounded by the insulating host, i.e., the microstructure of the two-component system is characterized by the so-called cermet topology. In the procedure discussed in Refs. 4 and 5, the coherent-potential approximation[6] (CPA) is employed in order to take into account the contributions to the local electric field arising from the randomly located polarizable particles. This theory therefore represents a self-consistent generalization of the Maxwell-Garnett[7] (MG) model which has been widely used to interpret the optical behavior of inhomogeneous systems. The disorder was shown to cause a sizable broadening and a red shift of absorption peaks. In contrast, the MG model assumes the local field acting on a particle to be given by the Lorentz relation, i.e., the presence of disorder is ignored. As has been noted in many experimental studies, the MG theory tends to underestimate the linewidths of absorption features and to place their positions at too-short wavelengths. The CPA treatment presented in Refs. 4 and 5 demonstrates that the randomness of the particle positions has pronounced influence on the optical properties of inhomogeneous media and that this effect can, at least partially, explain the discrepancies between the predictions of the MG model and observed absorption spectra.

The purpose of the present work is twofold: First, in Sec. II several features of the theory given in Refs. 4 and 5 are discussed in greater detail in order to illustrate the consequences of the coherent-potential approximation. In particular, the implications of the lattice-gas model, on which the theory is based, are demonstrated. Also, it is shown that the dielectric function of the composite derived within the CPA lies within the bounds which are known to exist on general grounds for any two-component system.[8–10] A comparison is then given of the CPA and an alternative method for treating particle interactions in random systems which has recently been proposed by Lamb *et al.*[11] This comparison also serves to illustrate the effect of multipole interactions on absorption spectra. Furthermore, the CPA treatment is extended to the case of particle mixtures embedded in a dielectric host, in order to study the influence of deviations from uniform particle size. Finally, the relationship of the theory given in Refs. 4 and 5 to its two-dimensional analog will be discussed. This is of particular importance for experiments on ultrathin inhomogeneous films which might consist of

 ©1984 The American Physical Society

only a single plane of particles suspended on a substrate material.

In all of the cases listed above, the dielectric properties of the metallic particles are for illustrative purposes represented by a Drude model. Applications to several real metals in dielectric hosts and comparisons with experimental spectra will be discussed in Sec. III. Such comparisons are necessarily of a qualitative nature since the present theoretical work deals only with one particular aspect of the optical properties of composites, namely, the influence of disorder. Real systems, on the other hand, are usually very difficult to characterize and their absorption spectra can be affected by a variety of factors such as nonrandom-particle distributions (particle clustering), deviations from spherical particle shape, nonuniform size, defects within particles, voids within the insulating medium, etc.

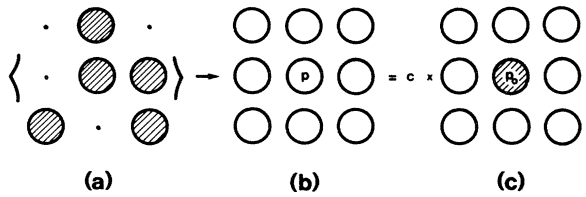

FIG. 1. (a) Schematic representation of a lattice gas for particles of polarizability $\alpha_0(\omega)$ (shaded circles). (b) Fully occupied lattice of "average particles" with effective polarizability $\alpha(\omega)$ (open circles). (c) Real impurity particle in otherwise perfect lattice of average particles. The CPA consists in identifying the induced-dipole moment $\vec{p}$ of a particle in (b) with that induced in impurity in (c), $\vec{p}_0$, weighted by impurity concentration c [see Eq. (6)].

II. THE COHERENT-POTENTIAL APPROXIMATION FOR TWO-COMPONENT SYSTEMS OF CERMET TOPOLOGY

A. Description of theory

Let us consider a system of identical metal particles of spherical shape (radius R) and dielectric function $\epsilon_0(\omega)$ embedded in a continuous insulating host material with dielectric function $\epsilon_1(\omega)$. The particle size is assumed to be small compared to the wavelength of the incident radiation. The polarizability of a single sphere surrounded by the medium is given by[12]

$$\alpha_0(\omega)=R^3\frac{\epsilon_0(\omega)-\epsilon_0(\omega)}{\epsilon_0(\omega)+2\epsilon_1(\omega)} . \tag{1}$$

In order to obtain an approximate expression for the macroscopic dielectric function $\epsilon(\omega)$ of the two-component system, we first replace the true random-particle distribution by a lattice gas. Thus the particles may only occupy the sites of a fictitious lattice. The symmetry of this lattice is assumed to be cubic (sc, bcc, fcc), and the lattice constant a is chosen such that the nearest-neighbor spacing d satisfies $d \geq 2R$. As we will demonstrate for a particular case in the following section, the choice of the lattice symmetry is not crucial because of the long-range nature of dipole interactions. However, most examples will be given for the fcc structure since it implies weaker geometrical constraints on the particle distributions than those for the bcc or sc lattices.

Let us assume a fraction c of sites of the hypothetical lattice to be occupied by metallic particles. This concentration c may vary between 0 and 1. It is related to the volume density of particles n and to the fraction of volume occupied by metal f by

$$n=c\frac{m}{a^3}=f\left[\frac{4\pi}{3}R^3\right]^{-1} , \tag{2}$$

where $m=1,2,4$ for sc, bcc, fcc, respectively. This partially occupied lattice will now be simulated by a fully occupied lattice of identical "average particles," each of which is characterized by an effective single-particle polarizability $\alpha(\omega)$. [See schematic views in Figs. 1(a) and 1(b).] Once a procedure is established for determining $\alpha(\omega)$, the dielectric function of the composite, $\epsilon(\omega)$, may be obtained via the Clausius-Mossotti (CM) relation:[13]

$$\frac{\epsilon(\omega)-\epsilon_1(\omega)}{\epsilon(\omega)+2\epsilon_1(\omega)}=\frac{4\pi}{3}\frac{m}{a^3}\alpha(\omega) . \tag{3}$$

[Note that $m/a^3=n/c$ represents the volume density of the effective particles with polarizability $\alpha(\omega)$.] Equation (3) is applicable since the average particles form a complete lattice of cubic symmetry.

The main task now consists in finding an adequate representation of the effective polarizability $\alpha(\omega)$. The most straightforward approximation of $\alpha(\omega)$ would be given by

$$\alpha(\omega)=c\alpha_0(\omega) \quad \text{(ATA)} . \tag{4}$$

This choice corresponds to the average—t-matrix approximation (ATA) in alloy theories. Inserting (4) into (3), we obtain the formula originally derived by Maxwell-Garnett to describe the optical properties of randomly dispersed metallic particles:[7]

$$\frac{\epsilon(\omega)-\epsilon_1(\omega)}{\epsilon(\omega)+2\epsilon_1(\omega)}=\frac{4\pi}{3}n\alpha_0(\omega) \quad \text{(MG)} . \tag{5}$$

Since the Clausius-Mossotti relation is strictly applicable to only cubic structures, the MG formula (5) neglects that contribution to the local electric field which arises from the randomly distributed metallic spheres in the vicinity of a given particle. In order to include these fields in an approximate manner, an improved representation of $\alpha(\omega)$ must be found.

Within the coherent-potential approximation the procedure for determining $\alpha(\omega)$ is as follows.[6,14] Let us assume first that the origin of the lattice is occupied by a real particle with polarizability $\alpha_0(\omega)$ and all other sites by average particles with polarizability $\alpha(\omega)$. The dipole moment induced in the particle at the origin due to an external field is defined as $\vec{p}_0$. If the origin is instead occupied by an average particle (all other sites as before), the

induced dipole moment is denoted by $\vec{p}$. The CPA then consists in identifying

$$\vec{p}=c\vec{p}_0 \tag{6}$$

$$\alpha(\omega)=c\alpha_0(\omega)\Big/\left[1+[\alpha_0(\omega)-\alpha(\omega)]\sum_{\vec{q}}\frac{U(\vec{q})}{1+\alpha(\omega)U(\vec{q})}\right] \quad \text{(CPA)} \tag{7}$$

where the sum over $\vec{q}$ extends over the Brillouin zone of volume $m(2\pi/a)^3$ and $U(\vec{q})$ denotes the Fourier transform of the dipole tensor:

$$U_{\nu\mu}(\vec{q})=\sum_{\vec{R}\ (\neq\vec{0})} e^{i\vec{q}\cdot\vec{R}}(R^2\delta_{\nu\mu}-3R_\nu R_\mu)R^{-5}\,. \tag{8}$$

Since we have assumed isotropic particles and cubic lattice symmetry, it can easily be shown that the average particles are also isotropic. Thus an explicit tensor notation in Eq. (7) has been omitted for convenience.

Obviously, if $U(\vec{q})$ is set equal to 0 in Eq. (7), we recover the average–t-matrix expression $\alpha(\omega)$ given in Eq. (4). Thus the local fields from randomly located polarizable particles which are neglected in the ATA and MG theory, appear in the CPA via the Brillouin-zone integration over the dipole tensor $U(\vec{q})$. In the case of a fully occupied cubic lattice, on the other hand, $c=1$ and $\alpha(\omega)=\alpha_0(\omega)$. In this limit only the small-$\vec{q}$ limit of $U(\vec{q})$ for transverse fields, $-\frac{4}{3}\pi n$, enters the expression for the dielectric function. This may be seen by rewriting the Clausius-Mossotti relation in the form

$$\frac{\epsilon(\omega)}{\epsilon_1(\omega)}-1=4\pi n\frac{\alpha_0(\omega)}{1-\frac{4}{3}\pi n\alpha_0(\omega)} \quad \text{(ATA)}\,. \tag{9}$$

[see schematic representation in Fig. 1(c)]. As shown in detail in Ref. 5 [see Eqs. (6)–(13) and Appendix], this equation leads to the following self-consistency condition for the effective polarizability $\alpha(\omega)$:

Thus the single-particle polarizability $\alpha_0(\omega)$ is renormalized via the interaction $U(\vec{q}_0)=-\frac{4}{3}\pi n$, where $\vec{q}_0$ corresponds to the wave vector of the incident radiation. The CPA, however, gives

$$\frac{\epsilon(\omega)}{\epsilon_1(\omega)}-1=4\pi n\frac{\alpha_0(\omega)/\gamma(\omega)}{1-\frac{4}{3}\pi n\alpha_0(\omega)/\gamma(\omega)} \quad \text{(CPA)}\,, \tag{10}$$

where $\gamma(\omega)$ denotes the denominator of Eq. (7). The single-particle polarizability $\alpha_0(\omega)$ is seen to be further renormalized by the factor $[\gamma(\omega)]^{-1}$ as a result of the positional disorder among the metal particles.

B. Application to Drude particles

In this section we apply the CPA to a system of Drude particles in order to illustrate the effect of the disorder on the absorption spectra and to examine more closely the validity of the lattice-gas model. As shown in Ref. 5, the interpretation of disorder-induced modifications of ab-

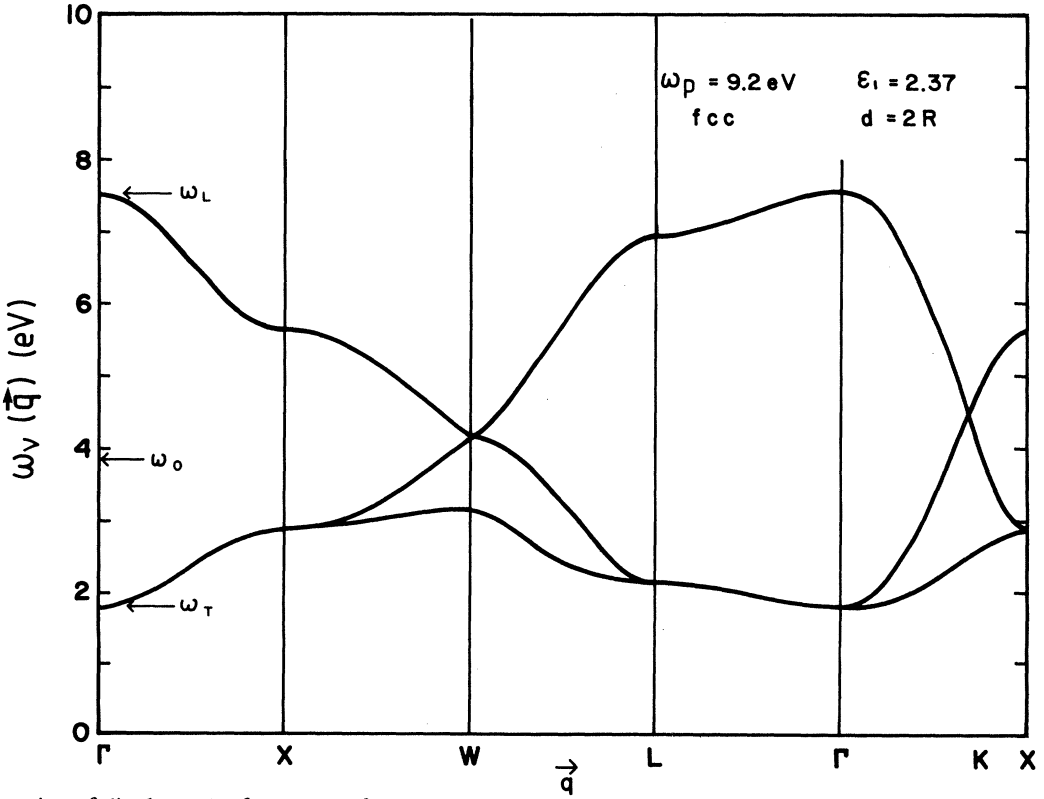

FIG. 2. Dispersion of dipole modes for ordered fcc lattice of Drude particles in dielectric medium. The single-particle resonance is ω_0 and the longitudinal and transverse modes at $\vec{q}=0$ are ω_L and ω_T, respectively.

sorption features is greatly facilitated by relating them to the normal modes of a fully occupied cubic lattice of metallic particles. If these particles are described by a Drude dielectric function, the modes are given by

$$\omega_\nu(\vec{q})=\omega_p \Big/ \left[1-\epsilon_1+\frac{3\epsilon_1}{1+\delta\lambda_\nu(\vec{q})}\right]^{1/2}, \quad \nu=1,\ldots,3 \tag{11}$$

where ω_p is the plasma frequency of the bulk metal, ϵ_1 (= const) is the dielectric constant of the surrounding medium, and the parameter δ is defined as

$$\delta=m(R/a)^3=R^3n/c=3f/4\pi c\ . \tag{12}$$

The functions $\lambda_\nu(\vec{q})$, $\nu=1,\ldots,3$, represent the eigenvalues of the renormalized dipole tensor

$$u_{\nu\mu}(\vec{q})\equiv\frac{a^3}{m}U_{\nu\mu}(\vec{q})\ . \tag{13}$$

Figure 2 shows the dispersion of $\omega_\nu(\vec{q})$ for the case of a fcc lattice with $\omega_p=9.2$ eV (corresponding to silver), $\epsilon_1=2.37$, and the nearest-neighbor distance is $d=2R$ (i.e., $a=2\sqrt{2}R$ and $\delta=\sqrt{2}/8$). Since the $\lambda_\nu(\vec{q})$ are confined to the interval $-\frac{4}{3}\pi\le\lambda_\nu\le\frac{8}{3}\pi$,[15] the frequencies $\omega_\nu(\vec{q})$ lie in the interval defined by

$$\omega_T=\frac{\omega_p}{(1+10.56\epsilon_1)^{1/2}}=1.80\text{ eV} \tag{14a}$$

and

$$\omega_L=\frac{\omega_p}{(1+0.21\epsilon_1)^{1/2}}=7.55\text{ eV}\ . \tag{14b}$$

These limiting frequencies correspond, respectively, to the transverse and longitudinal modes at $\vec{q}=\vec{0}$. The resonance frequency of an isolated Drude particle is given by

$$\omega_0=\frac{\omega_p}{(1+2\epsilon_1)^{1/2}}=3.84\text{ eV} \tag{15}$$

and corresponds to the value of $\omega_\nu(\vec{q})$ in the limit of van-

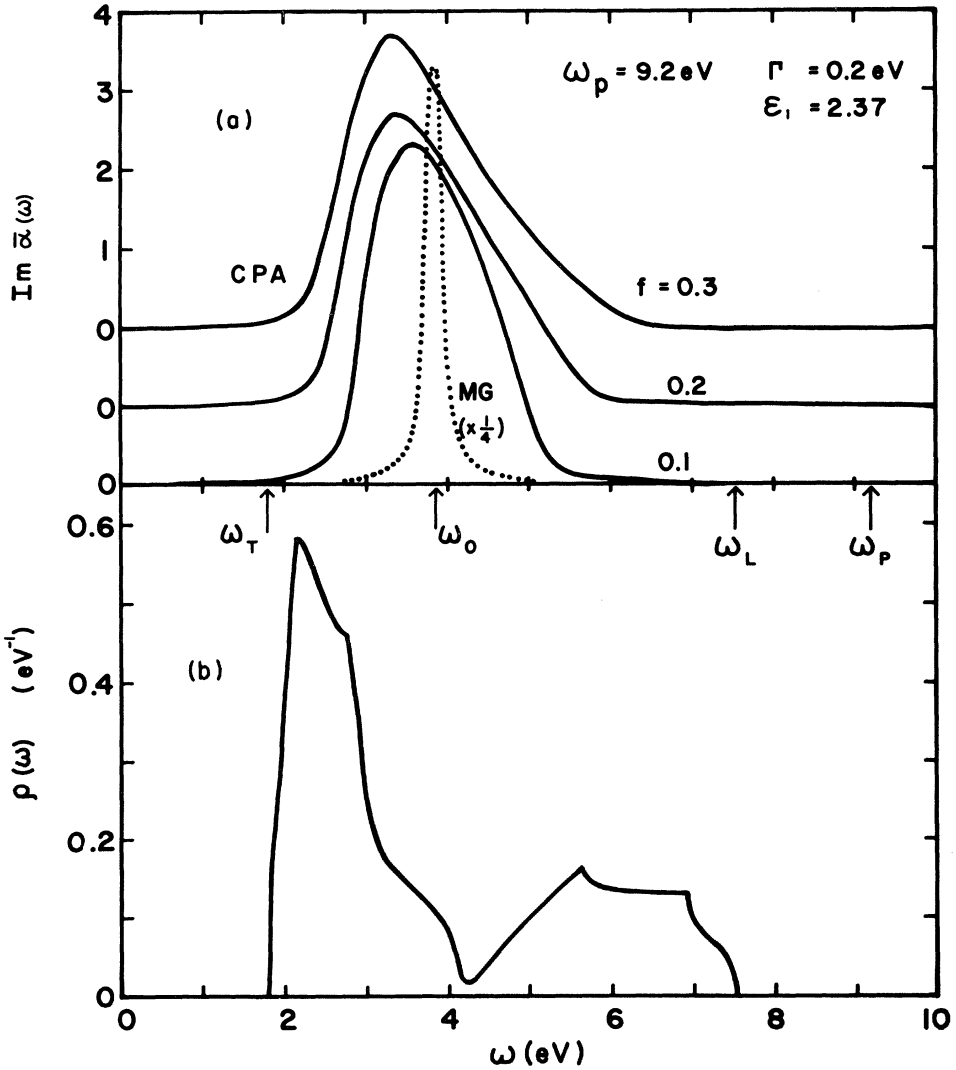

FIG. 3. (a) Frequency dependence of imaginary part of effective polarizability $\bar{\alpha}(\omega)$ at several filling fractions. Solid lines, CPA; dotted line, MG formula (independent of f). (b) Density of states for modes shown in Fig. 2.

ishing dipole interactions, i.e., $\lambda_\nu(\vec{q})\to 0$. It is useful to define the density of states for the normal modes $\omega_\nu(\vec{q})$ in the usual way:

$$\rho(\omega)=\frac{1}{3}\sum_{\nu=1}^{3}\sum_{\vec{q}}\delta(\omega-\omega_\nu(\vec{q}))\ . \tag{16}$$

The frequency dependence of $\rho(\omega)$ is shown in Fig. 3(b) for the same set of parameters as in the example given above.

It is illustrative to compare the effective polarizability $\alpha(\omega)$ of an average particle, obtained from the CPA self-consistency condition (7), with the corresponding ATA or MG result given by Eq. (5). To facilitate the comparison, we show in Fig. 3(a) the imaginary parts of the functions $\bar{\alpha}(\omega)=\alpha(\omega)/cR^3$ for three filling fractions, $f=0.1$, 0.2, and 0.3 [in the ATA we have from Eq. (4): $\bar{\alpha}(\omega)=\alpha_0(\omega)/R^3$ independently of f]. A damping parameter $\Gamma=0.2$ eV has been included in the Drude dielectric function of the metallic particles. Whereas in the MG approximation, $\mathrm{Im}\bar{\alpha}(\omega)$ is a symmetric peak of width Γ located at ω_0 independently of f, the CPA is seen to give a considerably broadened, asymmetric absorption feature whose maximum lies well below the single-particle frequency ω_0. Moreover, peak position and width depend strongly on the concentration of metallic particles.

The comparison of Figs. 3(a) and 3(b) indicates that, as a consequence of the disorder among particles, the effective polarizability $\alpha(\omega)$ shows spectral weight in the entire range of normal modes, $\omega_T\le\omega\le\omega_L$, which exist in the fully occupied three-dimensional lattice. (Because of the finite damping, weak absorption persists also beyond this frequency interval.) The degree to which the position and shape of $\mathrm{Im}\alpha(\omega)$ differ from the single-particle frequency ω_0 and width Γ, depends on the local electric fields produced by the surrounding randomly distributed particles, and therefore depends on the filling fraction f. Obviously, in the limit of small f, $\alpha(\omega)$ approaches the ATA or MG form given by $c\alpha_0(\omega)$. In the opposite limit of close packing (i.e., $c=1$ or $f=\pi\sqrt{2}/6$ for fcc), the effective polarizability $\alpha(\omega)$ also reduces to $\alpha_0(\omega)$, since, in the case of an ordered cubic lattice, the dipole fields of particles within the Lorentz cavity cancel each other identically.[13] A remarkable result of the CPA treatment of the disorder problem is that the induced broadening is largest at relatively small filling fractions: At $f=20\%$, $\mathrm{Im}\bar{\alpha}(\omega)$ has a width of 2 eV [full width at half maximum (FWHM)], i.e., an order of magnitude larger than in the ATA.

The fact that the maximum of the absorption peaks in Fig. 3(a) lies below the single-particle resonance frequency ω_0 is a direct consequence of the asymmetry of the density of states shown in 3(b). [A symmetric $\rho(\omega)$ would indeed lead to a symmetric broadening of $\alpha(\omega)$ about ω_0.] Since all three cubic structures sc, bcc, and fcc show very similar densities of states as a result of the long-range dipole interactions,[5] this kind of red shift presumably is a consequence of dipolar interactions in general and not just in the special case of a lattice-gas model.

Figure 4(a) shows the imaginary parts of the CPA dielectric function, $\epsilon(\omega)$, and of the corresponding loss function, $-\epsilon(\omega)^{-1}$, at several filling factors. The positions of the MG absorption and loss peaks are indicated by the vertical arrows. It can easily be verified that, in the MG limit, absorption as well as loss peaks have the same width Γ as the single-particle polarizability $\alpha_0(\omega)$, independently of f. In Fig. 4(b) the positions of absorption and loss peaks obtained using the CPA are plotted as functions of f. The vertical bars indicate the widths (FWHM). The absorption features predicted by the CPA are seen to lie typically 0.5 eV below the MG peaks while the positions of the loss features are blue-shifted by about the same amount. The disorder-induced broadening is

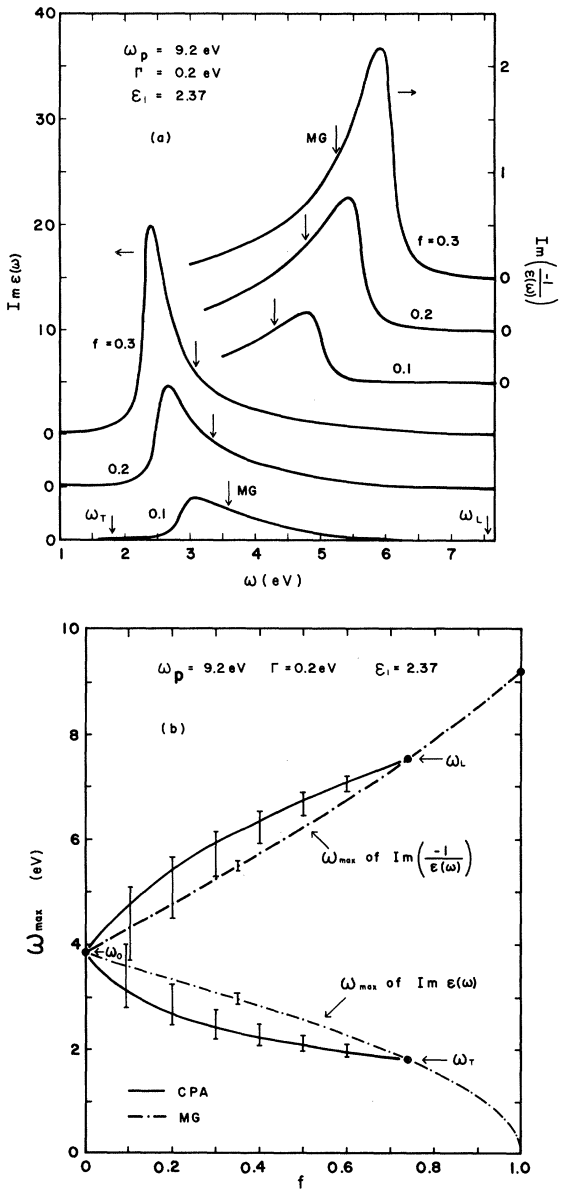

FIG. 4. (a) Absorption and loss spectra for Drude particles as calculated using CPA at various filling fractions. The corresponding peak positions in the MG limit are indicated by the arrows. (b) Variation of maxima of absorption and loss peaks with filling fraction. The vertical bars denote the width of these peaks (FWHM). In the MG limit, the width is equal to Γ regardless of f.

very pronounced and exceeds 1 eV for $f=10\%$ to 20%. In the limit of close packing ($c=1$ and $f=\pi\sqrt{2}/6$ in this example), the CPA approaches the MG limit, i.e., $\mathrm{Im}\epsilon(\omega)$ consists of a Lorentzian peak of width $\Gamma=0.2$ eV located at ω_T given by Eq. 14(a), while the maximum of $\mathrm{Im}[-\epsilon(\omega)^{-1}]$ is located at ω_L, Eq. 14(b). Thus in the case of a cubic, fully occupied lattice of particles, only the $\vec{q}=\vec{0}$ modes of the band structure shown in Fig. 2 contribute to the absorption and loss spectra. At smaller filling fractions, all (transverse as well as longitudinal) modes of the three-dimensional Brillouin zone, $\omega_T \le \omega_\nu(\vec{q}) \le \omega_L$, may contribute to the spectra as a consequence of the disorder.

The fact that the absorption peaks are red-shifted relative to the MG results while the loss peaks are blue-shifted may be understood as follows: Equations (9) and (10) for the composite dielectric function can be rewritten in the form

$$\frac{\epsilon(\omega)}{\epsilon_1}-1=\frac{3f\bar{\alpha}(\omega)}{1-f\bar{\alpha}(\omega)}\ , \tag{17}$$

where $\bar{\alpha}(\omega)=\alpha(\omega)/cR^3$ as in Fig. 3(b), and $\alpha(\omega)$ is given by expressions (4) and (7) in the ATA and CPA, respectively. With $\bar{\alpha}(\omega)=\bar{\alpha}_1(\omega)+i\bar{\alpha}_2(\omega)$ we obtain

$$\mathrm{Im}\epsilon(\omega)=\frac{3\epsilon_1 f\bar{\alpha}_2(\omega)}{[1-f\bar{\alpha}_1(\omega)]^2+[f\bar{\alpha}_2(\omega)]^2}\ , \tag{18}$$

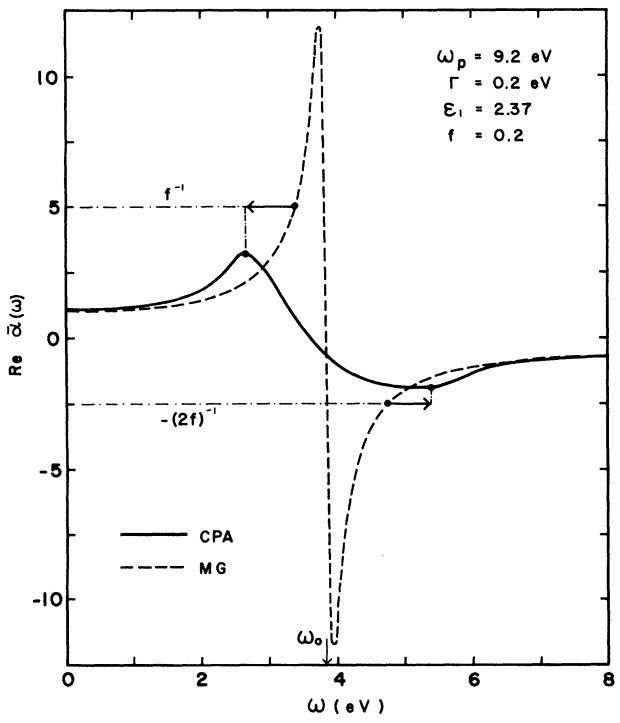

FIG. 5. Frequency dependence of real part of effective polarizability $\bar{\alpha}(\omega)$ for $f=0.2$. The intersections with or closest approaches to the lines $1/f$ and $-1/2f$ give the positions of the absorption and loss peaks, respectively [see Eqs. (18) and (19)]. The horizontal arrows indicate the frequency shifts of these peaks as a result of the disorder.

$$\mathrm{Im}\frac{-1}{\epsilon(\omega)}=\frac{3\epsilon_1 f\bar{\alpha}_2(\omega)}{[1+2f\bar{\alpha}_1(\omega)]^2+[2f\bar{\alpha}_2(\omega)]^2}\ . \tag{19}$$

Figure 5 shows the functions $\alpha_1(\omega)$ for $f=0.2$ obtained by applying the ATA and CPA. [The corresponding imaginary parts $\bar{\alpha}_2(\omega)$ are shown in Fig. 3(a).] The maxima of $\mathrm{Im}\epsilon(\omega)$ are approximately determined by the condition $|1-f\bar{\alpha}_1(\omega)|=\min$ whereas those of $\mathrm{Im}[-\epsilon(\omega)^{-1}]$ are given by $|1+2f\bar{\alpha}_1(\omega)|=\min$ [see dotted-dashed lines; the actual maxima of the absorption and loss peaks might differ somewhat from these positions because of the frequency dependence of the imaginary parts $\bar{\alpha}_2(\omega)$]. Evidently because of the disorder-induced broadening of $\mathrm{Im}\bar{\alpha}(\omega)$ [see Fig. 3(a)], the real part of the CPA effective polarizability, $\bar{\alpha}_1(\omega)$, approaches the lines f^{-1} and $-(2f)^{-1}$ much farther away from ω_0 than in the case of the ATA. This explains the red shift of the absorption peaks and blue shift of the loss peaks shown in Fig. 4.

C. The lattice-gas model

The application of the coherent-potential approximation to the disordered system of metal particles, as described in Sec. II A, is based on the lattice-gas model, i.e., on the restriction of the particle positions to the sites of an imagined (cubic) lattice. Obviously the choice of the lattice parameter (in relation to the particle diameter) as well as the symmetry of the lattice (sc, bcc, fcc) are, to some extent arbitrary and in order for the lattice-gas model to be justified, they should not influence the calculated absorption spectra as far as the overall qualitative behavior is concerned.

The essential physical argument for the adequacy of the lattice gas in the present problem is the fact that the dipole interaction is rather long ranged. Of course, with increasing interparticle spacings, the change of the local electric field due to the surrounding randomly distributed metal particles must diminish. However, because of the r^{-3} dependence of the dipole field, this reduction can be expected to be rather gradual. The symmetry of the fictitious lattice should have an even weaker influence on the effective local field at a given particle, at least as long as

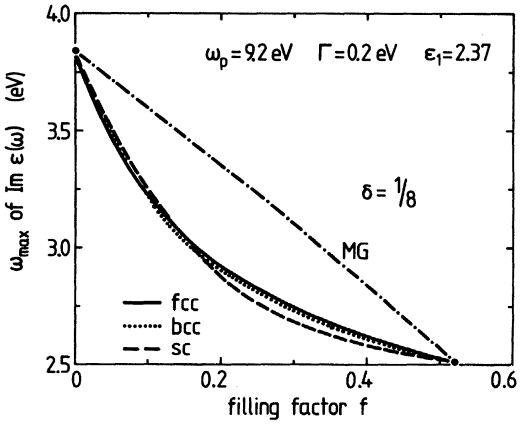

FIG. 6. Frequency of maximum of absorption peak as function of filling factor for sc, bcc, and fcc lattice gases. Interparticle spacings are chosen such that $\delta=\frac{1}{8}$ [see Eq. (12)].

the radial distribution of particles is not altered significantly.

The fact that the lattice symmetry plays only a minor role is already apparent from the remarkable similarity of the $\vec{q}$ dependence of the normal modes, $\omega_\nu(\vec{q})$, and, consequently, of the density of states, $\rho(\omega)$, for the completely occupied sc, bcc, and fcc lattices. (See Ref. 5 for a comparison of the densities of eigenvalues $\lambda_\nu(\vec{q})$ of the renormalized dipole tensor, $u_{\nu\mu}(\vec{q})$, Eq. (13), for these three lattices.) To illustrate this point further, we show in Fig. 6 the position of the main absorption peak as a function of filling factor as calculated within the CPA for sc, bcc, and fcc. The lattice parameter for sc corresponds to touching spheres (i.e., $a=d=2R$), while those for bcc and fcc have been slightly increased relative to the touching sphere spacings in order to compensate for the higher packing densities in these lattices. We chose

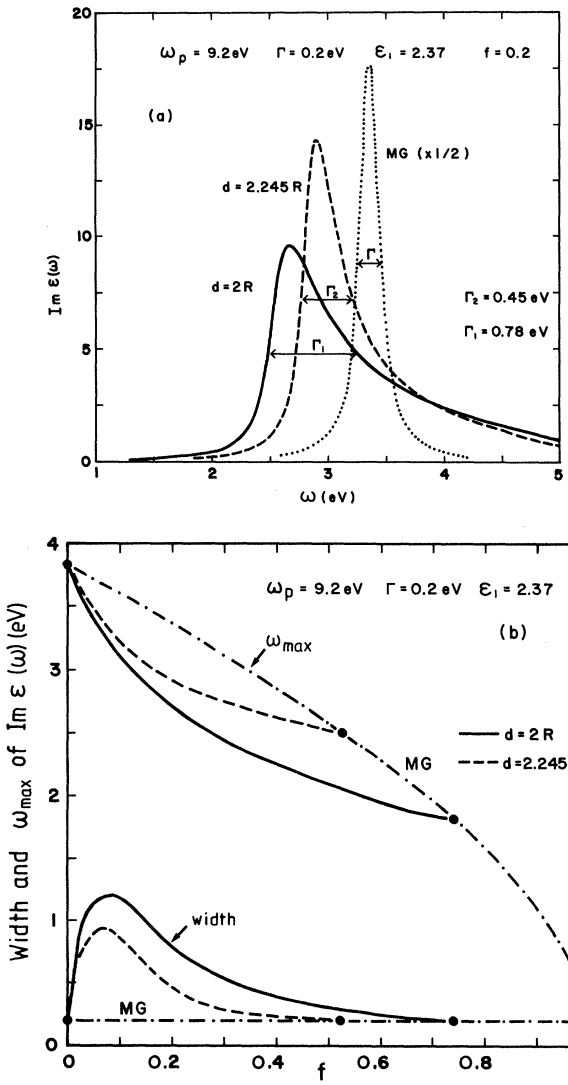

FIG. 7. (a) Imaginary part of composite dielectric function for fcc lattice gas of Drude particles as function of frequency. Nearest-neighbor distances d are indicated in the figure. (b) Variation of maximum and width of absorption peak as function of filling fraction. Nearest-neighbor spacings as in (a).

$d/R=(6\sqrt{3})^{1/3}=2.182$ for bcc and $d/R=(8\sqrt{2})^{1/2}=2.245$ for fcc so that $0.25a_{\rm fcc}^3=0.5a_{\rm bcc}^3=a_{\rm sc}^3=8R^3$. From Eq. (12) it follows that $\delta=\frac{1}{8}$ or $f=c\pi/6$ for all three lattices. Identical volume fillings therefore imply identical fractions of occupied sites for the three lattice symmetries. (Note that the maximum filling fraction for fcc is now $\pi/6$ and not $\sqrt{2}\pi/6$ as in the examples given in Figs. 2–5). The striking similarity of the peak positions shown in Fig. 6 demonstrates that the angular distribution of particle positions indeed plays only an insignificant role.

Let us now investigate the influence of the lattice parameter on the absorption spectra. Figure 7(a) shows a comparison of two spectra for the fcc lattice ($f=0.2$) with $d=2R$ ($\delta=\sqrt{2}/8$) as in Fig. 4(a) and $d=2.245R$ ($\delta=\frac{1}{8}$). Since the volume filling is chosen to be the same in both examples, the fraction of occupied sites is accordingly higher in the latter case ($c=0.38$ compared to 0.27). As a result of the larger average spacings between particles the disorder-induced red shift of the absorption peak as well as its width are diminished.

Figure 7(b) shows the positions and widths for these two geometries as a function of f. At volume fillings near 5–10%, the red shift and broadening are nearly the same for both spacings, whereas towards higher f values, the spectra for $d=2.245R$ approach more rapidly the Maxwell-Garnett limit. Since the concentration of occupied sites is always greater in the case of the larger lattice constant, one tends to be closer to the situation of a fully occupied lattice, where the dipole fields from neighboring particles cancel identically. As in the example given in Fig. 6, this limit is reached at $f=\pi/6$ for $d=2.245$ instead of at $\pi\sqrt{2}/6$ in the more realistic case of close packing, $d=2R$.

D. Bounds on composite dielectric function

The effective dielectric function $\epsilon(\omega)$ of an isotropic inhomogeneous medium is known to be limited in the complex ϵ plane by certain rigorous bounds irrespective of the topology of the medium.[8–10] For a two-component system of the kind discussed in this work these bounds are defined by the functions

$$E(x)=\epsilon_1\left[1-\frac{f(s-x)}{s[s-x-(1-f)/3]}\right] \tag{20}$$

and

$$E'(x)=\epsilon_1\left[1-\frac{f(s-x')}{s[s-x'-(1-f)/3]+(x'-\frac{2}{3})(1-f)}\right], \tag{21}$$

where $s=\epsilon_1/[\epsilon_1-\epsilon_0(\omega)]$, $x'=1-x/2$, and $0\le x\le\frac{2}{3}$.

$E(x)$ and $E'(x)$ describe two circular arcs which intersect at the end points, i.e., $E(0)=E'(0)$ and $E(\frac{2}{3})=E'(\frac{2}{3})$. It is easily shown that the former point coincides with the MG value of the dielectric function:

$$\epsilon(\omega)=\epsilon_1\frac{\epsilon_0(\omega)(1+2f)+2\epsilon_1(1-f)}{\epsilon_0(\omega)(1-f)+\epsilon_1(2+f)}=E(0)\,, \tag{22}$$

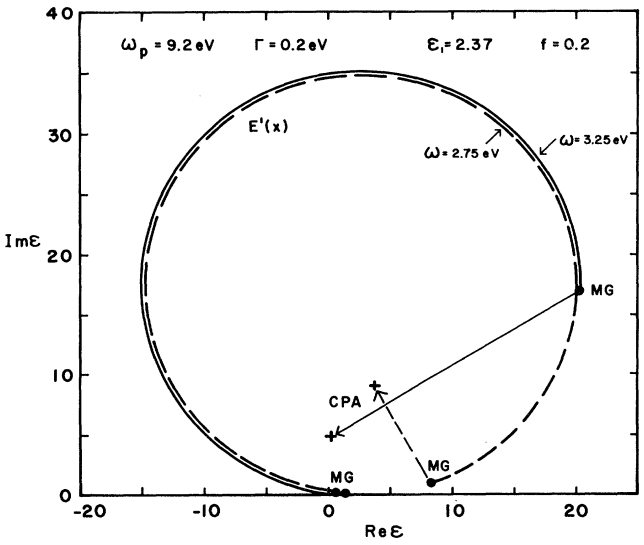

FIG. 8. Bounds of dielectric function $E'(x)$, Eq. (21), for two energies ω. The Maxwell-Garnett values are indicated by dots, the corresponding CPA results by crosses.

while the latter point corresponds to the MG dielectric function of the "inverse" topology (a volume fraction $1-f$ occupied by dielectric spheres surrounded by metallic medium):

$$\epsilon'(\omega)=\epsilon_0(\omega)\frac{\epsilon_1(3-2f)+2\epsilon_0(\omega)f}{\epsilon_1 f+\epsilon_0(\omega)(3-f)}=E(\tfrac{2}{3})\,. \tag{23}$$

Figure 8 shows the function $E'(x)$ at two frequencies, $\omega=2.75$ eV and $\omega=3.25$ eV, for $f=0.2$ [see spectra in Figs. 4(a) and 7(a)]. The dots mark the positions of the end points given by Eqs. (22) and (23). For clarity we do not show the arcs defined by $E(x)$ since they lie outside the area enclosed by $E'(x)$ and the straight line connecting the points $E(0)$ and $E(\frac{2}{3})$. At both energies, the values of the CPA dielectric function (crosses) lie well inside the boundaries, although their locations in the complex plane are rather different from the corresponding MG values. This behavior is fairly typical for other frequencies and filling fractions; in all the cases that we have investigated the CPA results were found to satisfy the required boundary conditions. On the other hand, they are not closely correlated with the corresponding MG limits even though the underlying microstructure is the same. In general, the CPA results tend to be much more concentrated near the origin of the complex ϵ plane since the disorder-induced broadening suppresses the rapid variations of $\mathrm{Im}\epsilon(\omega)$ shown by the MG dielectric function in the vicinity of the absorption-resonance frequency.

E. Multipole interactions

The results summarized in Fig. 4(b) demonstrate that the disorder-induced shift and broadening of absorption as well as loss peaks is largest at filling fractions near 10—20%. This behavior is in striking contrast to the effects that arise as a result of multipole interactions, which are not included in this work. In general, higher-than-

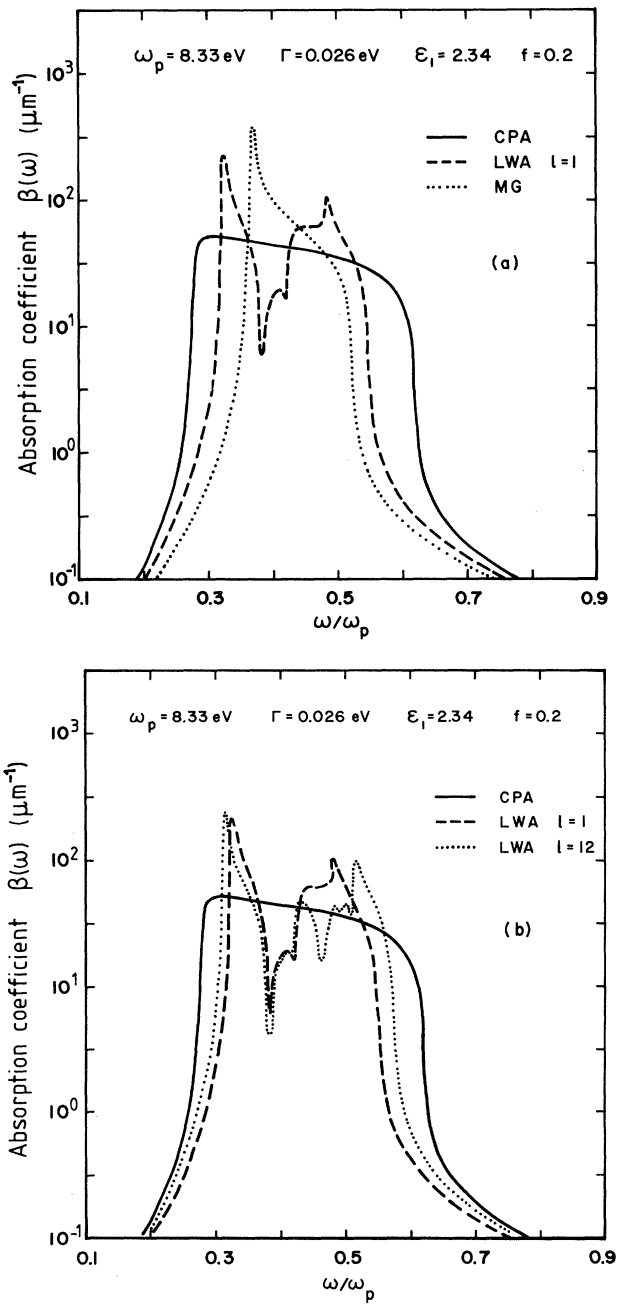

FIG. 9. Absorption coefficient (Drude) for gold particles in KBr. (a) Dipole approximation. Solid line, CPA; dashed line, theoretical results of Lamb *et al.* (Ref. 11); dotted line, Maxwell-Garnett formula. (b) Comparison of dipole approximation (solid line, CPA; dashed line, LWA) with multipole expansion (dotted line) of LWA (Ref. 11).

dipole terms become important at small interparticle spacings, i.e., at rather large values of f.[16]

In order to illustrate the role of multipole fields in absorption spectra we compare our results in this section with those of Lamb, Wood, and Ashcroft[11,17] (LWA), who investigated the optical properties of inhomogeneous systems using a rather different approach. Essentially, these authors replace the system of disordered particles by a periodic system with a large basis and describe the

random-particle arrangement within the unit cell in terms of distribution functions of a hard-sphere fluid. Figure 9(a) shows a comparison of the absorption coefficient $\beta(\omega)$ for gold particles (represented for simplicity by a Drude dielectric function) in KBr as calculated by LWA in the dipole limit (multipole index $l=1$) and the corresponding result obtained using the CPA. Although the quantitative details are quite different for the two approaches, the overall behavior is similar. Compared to the Maxwell-Garnett limit, the disorder in both theories is seen to cause a red shift and a broadening of the absorption peak. Since the numerical work of LWA includes only specific interparticle correlations of a hard-sphere distribution, the absorption coefficient exhibits considerable fine structure. The CPA, on the other hand, is known to represent an average over many (including higher order) particle distributions; thus the red shift and broadening are more pronounced.

LWA have also calculated the absorption spectrum including higher-order multipole interactions between particles. A comparison of their results for $l=1$ and $l\leq 12$ with the CPA is shown in Fig. 9(b). The multipoles are seen to increase the amount of fine structure in the absorption coefficient and to enhance the red shift of the main absorption peak near $\omega=0.32\omega_p$. While some of the new features correspond to genuine multipole resonances, others are certainly a consequence of the particular interparticle distributions included in the theory. (The pronounced dip at $\omega=0.38\omega_p$, for example, is presumably spurious since it is also present in the dipole limit.) Note also that the damping constant Γ in Fig. 9 corresponds to the bulk value of gold. If a more realistic value is used to take into account the finite particle size, much of the fine structure disappears and the broadening of the absorption peak increases. (See Figs. 3 and 4 of Ref. 11.) In this case the similarity of the results for $l=1$ and $l\leq 12$ is much greater than in the example shown in Fig. 9(b).

The absorption spectra in Fig. 9 are for a rather small filling fraction of 20%. At these concentrations the average spacing between metal particles is apparently sufficiently large so that multipole fields cause only minor modifications of the position and shape of the absorption peak. At smaller values of f, these effects are even weaker. The disorder among particles, on the other hand, causes strong deviations from the Maxwell-Garnett result, even at filling fractions as small as 5—10 % (see Fig. 4).

The role of multipole interactions has also been investigated by Doyle[18] for ordered cubic lattices of perfectly conducting spheres. While multipole effects are weaker in ordered than in disordered systems (the latter involves more close approaches between particles), it is nevertheless instructive to compare them with the disorder-related changes of the dielectric function. In Fig. 10 the enhancement of ϵ compared to the MG value is plotted as function of filling fraction. The solid line gives the result obtained within the CPA (dipoles only) for a lattice gas (fcc symmetry) where the lattice parameter is kept constant ($a=4R/\sqrt{3}$). The dashed line corresponds to the increase of ϵ due to multipoles in the case of an ordered fcc lattice where the lattice constant is varied according to $f=m\frac{4}{3}\pi(R/a)^3$ [see Eq. (12); $c=1$ in this case since the lattice is fully occupied].[18] The latter increase is seen to become important only at $f\geq 50\%$, while the enhancement due to disorder is appreciable already near $f=10\%$ to 20%. (Since the CPA calculation includes only dipole fields, $\epsilon=\epsilon_{\mathrm{MG}}$ at $f_{\max}=0.74$. Multipole interactions, on the other hand, cause ϵ to diverge at $f_{\max}$.)

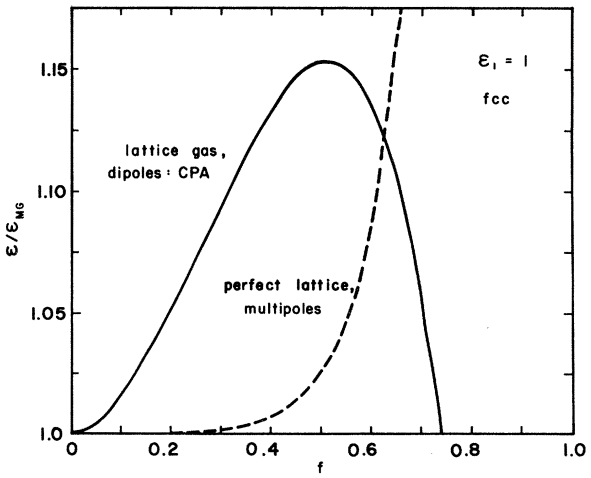

FIG. 10. Enhancement of Maxwell-Garnett dielectric constant for perfectly conducting spheres in vacuum as function of filling fraction. Solid curve: effect of disorder for lattice gas as calculated within CPA, dashed curve: influence of multipoles for perfectly ordered fcc lattice (Ref. 18).

F. Multicomponent systems: nonuniform particle size

In the work discussed so far we have assumed that all metal particles are spherical and of identical size. In practice, of course, deviations from exact sphericity and from uniform size are nearly always present, so that true inhomogeneous systems consisting of metal particles in a dielectric medium are in fact usually multicomponent systems. The CPA treatment described in Sec. II A can easily be extended to composites of this kind. As an example, we discuss in this section a random distribution of spherical particles whose dielectric properties are assumed to be identical [i.e., they are characterized by the same $\epsilon_0(\omega)$], but whose radii may be different.

Let us introduce the parameters $\gamma_i=(R_i/R)^3$, where R_i is the radius of the ith type of particle and R the radius of the average particle whose effective polarizability $\alpha(\omega)$ will be calculated using the CPA. Since the dielectric functions are assumed to be the same for all particles, the single-particle polarizabilities may be written as

$$\alpha_i(\omega)=R_i^3\frac{\epsilon_0(\omega)-\epsilon_1}{\epsilon_0(\omega)+2\epsilon_1}=\gamma_i\alpha_0(\omega)\ . \tag{24}$$

As in the case of the two-component system, we first calculate the induced dipole moment $\vec{p}_i$ of a real particle of radius R_i surrounded by a perfect fcc lattice of ficticious particles of radius R and polarizability $\alpha(\omega)$. If the relative concentrations of the various types of particles are

denoted by c_i we have, in analogy to Eq. (6),

$$\vec{p}=\sum_i c_i \vec{p}_i \ , \tag{25}$$

where $\vec{p}$ is again the dipole moment induced in an average particle. Instead of Eq.(7), therefore, we obtain the following self-consistency condition for the effective polarizability $\alpha(\omega)$:

$$\alpha(\omega)=\sum_i c_i \alpha_i(\omega) \Big/ \left[1+[\alpha_i(\omega)-\alpha(\omega)]\sum_{\vec{q}} \frac{U(\vec{q})}{1+\alpha(\omega)U(\vec{q})}\right] . \tag{26}$$

(This formula is, of course, also applicable to inhomogeneous systems consisting of particles whose shapes and/or dielectric properties are nonuniform.)

In order to illustrate the consequences of nonuniform particle sizes we show in Fig. 11 absorption spectra for silver particles (represented by a Drude model as before) with the following distributions: (a) Equal volume fractions (10%) are occupied by particles of radius $R_1=R$ and $R_2=R/2^{1/3}$, i.e., $f_1=f_2=0.1$ and $\gamma_1=1.0$, $\gamma_2=0.5$. The concentrations of sites in the fcc lattice that are occupied by these two types of particles are, respectively, $c_1=f_1(\frac{4}{3}\pi\delta\gamma_1)^{-1}=0.135$ and $c_2=2c_1$. (b) Equal concentrations of sites are occupied by particles of radius $R_1=R$ and $R_2=R/2^{1/3}$, i.e., $\gamma_1=1.0$, $\gamma_2=0.5$ as in (a), but $f_1=0.4/3$ and $f_2=0.2/3$ ($c_1=c_2=0.18$). The total filling fraction $f=f_1+f_2$ is 0.2 in both cases. Also shown for comparison is the absorption spectrum for particles of uniform size (radius R) at $f=0.2$ [see also Fig. 4(a)].

The nonuniformity of particle sizes is seen to enhance the broadening of the absorption peak while the red shift of the maximum relative to the MG position (see arrow) is slightly reduced. This may be understood by considering the spectra for $R_1\neq R_2$ as approximate superpositions of absorption peaks corresponding to filling fractions f_1 and f_2. According to Fig. 4(b), the broadening is larger for $f=0.2/3$, $0.3/3$, $0.4/3$ than for $f=0.2$, while the maxima of the absorption peaks lie at higher energies in this range of f. Since the MG formula, on the other hand, depends only on the total volume fraction occupied by metal (in our example all particles are assumed to have identical dielectric properties), it yields identical peaks of width $\Gamma=0.2$ eV for all three cases shown in Fig. 11.

G. Two-dimensional inhomogeneous systems

As pointed out in Sec. II A, in a three-dimensional random-particle distribution the effective polarizability

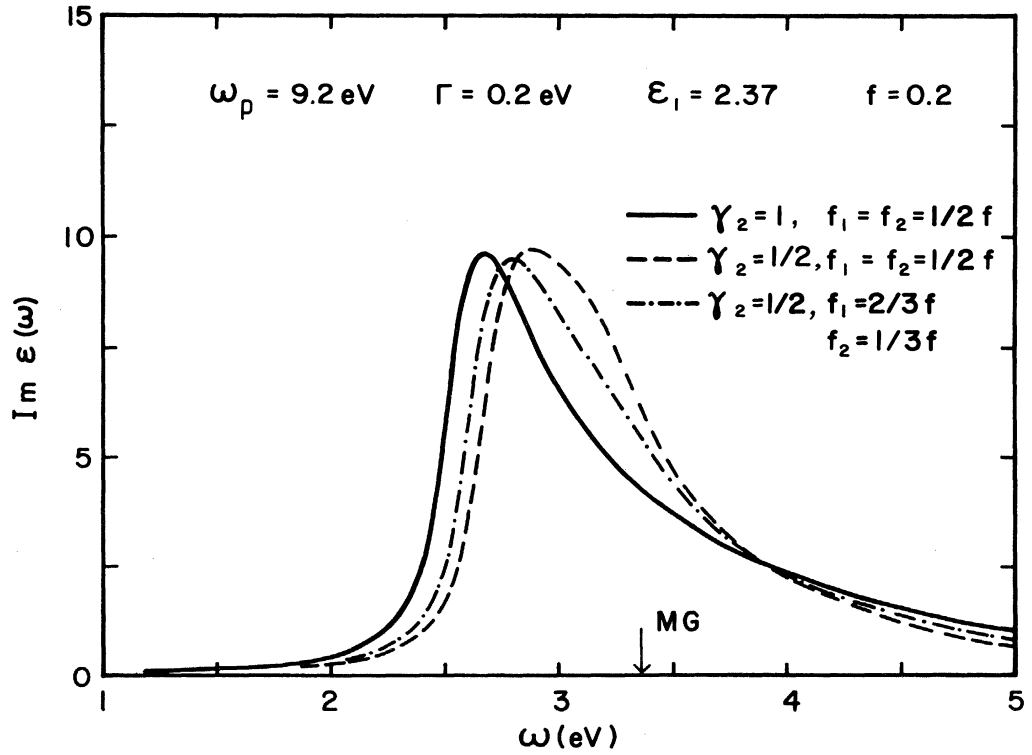

FIG. 11. Absorption peak for various mixtures of Drude particles of nonuniform size [$\gamma_i=(R_i/R)^{-3}$, f_i equals partial filling fractions; see text]. In the Maxwell-Garnett approximation, all three mixtures give a Lorentzian peak of width Γ at the position marked by the arrow.

$\alpha(\omega)$ of an average particle is isotropic if the polarizabilities $\alpha_0(\omega)$ of the individual real particles are isotropic. Some measurements on inhomogeneous systems, however, have been performed for ultrathin films which might contain only a single plane of particles suspended on a transparent substrate. The purpose of this section is to discuss the modifications of the theory described above in the case of a two-dimensional random arrangement of particles. Only the main features are presented; a more complete analysis of this problem is given elsewhere.[19]

Let us consider at first a fully occupied square lattice of identical Drude particles of polarizability $\alpha_0(\omega)$. (The surrounding medium is taken to be vacuum for simplicity.) As a consequence of dipole interactions, the total polarizability for this system is given by

$$\vec{\vec{\alpha}}(\vec{q},\omega)=\frac{\alpha_0(\omega)}{\vec{\vec{1}}+\alpha_0(\omega)\vec{\vec{U}}(\vec{q})}\,, \tag{27}$$

where $\vec{\vec{U}}(\vec{q})$ is defined as in (8) except that the sum over sites is now two dimensional. In the long-wavelength limit ($qa \ll 1$, where a is the lattice constant), $\vec{\vec{U}}(\vec{q})$ is diagonal with elements U_0 and $-0.5U_0$, where $U_0=9.03a^{-3}$. The lattice polarizability (27) exhibits two resonances at frequencies $\omega_{||}=\omega_0(1-0.5R^3U_0)^{1/2}$ (doubly degenerate) and $\omega_\perp=\omega_0(1+R^3U_0)^{1/2}$. $\omega_0=\omega_p/\sqrt{3}$ is the single-particle resonance frequency. The width of $\mathrm{Im}\vec{\vec{\alpha}}(\vec{0},\omega)$ is easily shown to be equal to Γ, the damping constant of the particle dielectric function.

In order to apply the CPA to the two-dimensional disordered system, the true particle distribution is again simulated by a lattice gas, i.e., the particle positions are confined to the sites of a fictitious square lattice. Let us denote by $\vec{p}_0$ the induced-dipole moment of a real particle surrounded by a fully occupied lattice of average particles of effective polarizability $\vec{\vec{\alpha}}(\omega)$. If the site at the origin is instead occupied by an average particle, its induced-dipole moment is $\vec{p}$. The CPA consists now in identifying

$$\vec{p}=c\vec{p}_0\,, \tag{28}$$

where c is the concentration of occupied sites. In complete analogy to Eq. (7) this relation leads to the following self-consistency condition for $\vec{\vec{\alpha}}(\omega)$:

$$\vec{\vec{\alpha}}(\omega)=c\alpha_0(\omega)\Big/\left[\vec{\vec{1}}+[\alpha_0(\omega)\vec{\vec{1}}-\vec{\vec{\alpha}}(\omega)]\sum_{\vec{q}}\frac{\vec{\vec{U}}(\vec{q})}{\vec{\vec{1}}+\vec{\vec{\alpha}}(\omega)\cdot\vec{\vec{U}}(\vec{q})}\right]\,, \tag{29}$$

where the sum over $\vec{q}$ extends over the two-dimensional Brillouin zone.

Since the average particles form an ordered, fully occupied lattice, the total polarizability for this sytem is given by

$$\vec{\vec{\alpha}}(\vec{q},\omega)=\frac{\vec{\vec{\alpha}}(\omega)}{\vec{\vec{1}}+\vec{\vec{\alpha}}(\omega)\cdot\vec{\vec{U}}(\vec{q})}\quad\text{(CPA)}\,. \tag{30}$$

It can be shown that $\vec{\vec{\alpha}}(\omega)$ is in fact diagonal with elements $\alpha_{||}(\omega)$ (doubly degenerate) and $\alpha_\perp(\omega)$. Thus, even though the original particles have an isotropic polarizability $\alpha_0(\omega)$, the average particles are anisotropic because of the symmetry of the dipole interactions included in the denominator of Eq. (29). The disorder accordingly influences the modes parallel and perpendicular to the plane of particles in a different manner. If the effect of the random dipole fields in Eq. (29) is neglected, we obtain the approximation corresponding to the ATA, $\alpha(\omega)=c\alpha_0(\omega)$. The total polarizability in this limit is given by

$$\vec{\vec{\alpha}}(\vec{q},\omega)=\frac{c\alpha_0(\omega)}{\vec{\vec{1}}+c\alpha_0(\omega)\vec{\vec{U}}(\vec{q})}\,,\quad\text{(ATA)} \tag{31}$$

which, in the long-wavelength limit, shows two resonances at frequencies $\omega_{||}=\omega_0(1-0.5cR^3U_0)^{1/2}$ (doubly degenerate) and $\omega_\perp=\omega_0(1+cR^3U_0)^{1/2}$. The width of these peaks is easily shown to be given by Γ. In the ATA, therefore, the absorption frequency of the parallel mode shifts smoothly as function of concentration from ω_0 at $c=0$ to $\omega_0-\Delta\omega_0$ in the case of a full monolayer where $\Delta\omega_0\equiv 0.25R^3U_0\omega_0$. The perpendicular mode shifts upward from ω_0 to $\omega_0+2\Delta\omega_0$. The disorder at finite concentrations has no effect on the shapes or widths of the absorption peaks in this approximation.

Figure 12(a) shows the imaginary parts of $\bar{\alpha}_{||}(\omega)$ and $\bar{\alpha}_\perp(\omega)$ which are defined as the diagonal components of $\vec{\vec{\alpha}}(\vec{0},\omega)R^{-3}$ as calculated within the CPA. The corresponding peaks in the ATA are located at $\omega_{||}=3.94$ eV and $\omega_\perp=4.11$ eV (the single-particle frequency is $\omega_0=4$ eV). The disorder is seen to cause a red shift of about 1 eV of the parallel mode and an equally strong blue shift of the perpendicular mode. Both absorption peaks are in addition broadened and have asymmetric line shapes. A remarkable feature of these spectra is the fact that the disorder-induced width of the parallel mode is significantly larger than that of the perpendicular mode. This effect may be understood by considering the disordered system as an assembly of clusters of different sizes and configurations. In general, the parallel modes of these clusters differ more widely than the perpendicular modes. Thus the distribution of parallel modes in a disordered system will be much broader than that of the perpendicular modes.

Evidence for this effect can be found in recent experiments by Yamaguchi *et al.*[20] Figure 12(b) shows a typical absorption spectrum for small silver particles suspended on a transparent film of polyvinyl alcohol. The separation into parallel and perpendicular components of the spectrum is achieved by varying the angle of incidence of the radiation. The parallel mode is seen to be considerably broader than the perpendicular mode, in qualitative agreement with the theoretical spectra shown in Fig. 12(a). A detailed comparison with the CPA results in 12(a) is, of course, not possible since the measured spectra

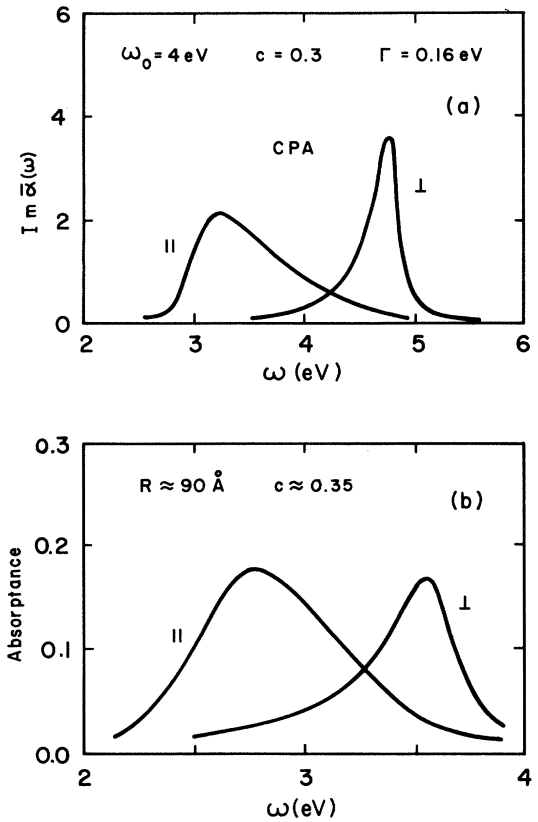

FIG. 12. Imaginary parts of parallel and perpendicular components of polarizability $\bar{\alpha}(\omega)=\vec{\alpha}(\vec{0},\omega)R^{-3}$, Eq. (30), for two-dimensional lattice gas ($c=0.3$) of Drude particles as calculated within CPA. (b) Measured absorption spectra for layer of silver particles (radius ≈ 90 Å, concentration $c \approx 35\%$) randomly distributed on sheet of polyvinyl alcohol (Ref. 20).

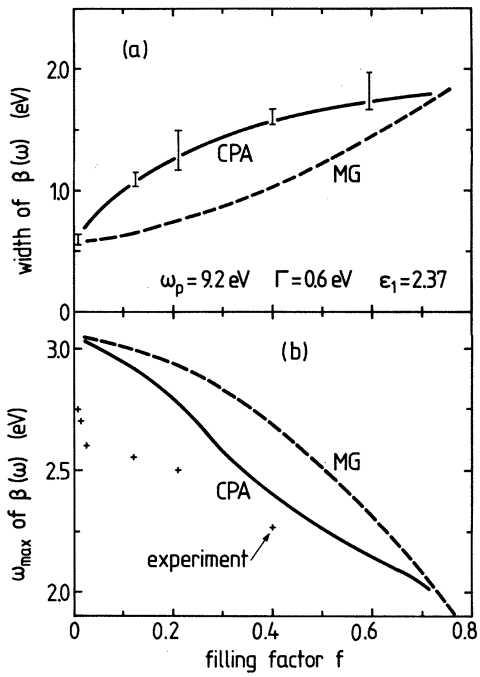

FIG. 13. (a) Width and (b) position of absorption peaks for silver particles in gelatin ($\epsilon_1=2.37$) as functions of filling fraction. Solid lines, CPA; dashed lines, MG approximation. Experimental results are indicated by vertical bars and crosses (Ref. 21).

are also influenced by a variety of other effects such as interband transitions and image fields. The influence of the disorder among particles, however, is clearly visible in the experimental data.

III. APPLICATIONS AND COMPARISON WITH EXPERIMENTS

In this section we present applications of the CPA to several real inhomogeneous systems where the metal particles are described by the appropriate dielectric functions. Although any comparison with experimental absorption data is necessarily of a qualitative nature at this stage, we believe there is evidence for the kind of disorder-induced spectral changes which we have described in the preceding section.

In Fig. 13(a) a comparison is given of the calculated and measured[21] width of the absorption coefficient for silver particles at various concentrations in a gelatin medium. The bulk dielectric function[22] of Ag is used for the particles with a free-electron damping of $\Gamma=0.6$ eV. This rather large value was deduced from spectra at very low Ag concentrations and seems to be caused by imperfections within the particles. The measured widths are seen to increase with increasing filling fraction up to more than 1.5 eV. Both the overall magnitude and the trend of this broadening are very well described by the CPA whereas the Maxwell-Garnett fomula systematically underestimates the peak width by about 0.4—0.5 eV. The comparison of the peak positions is shown in Fig. 13(b). Here, the data shows a large amount of scatter, in particular, near $f \lesssim 5\%$. These wide variations of ω_{max} are presumably related to particle clustering which is not in-

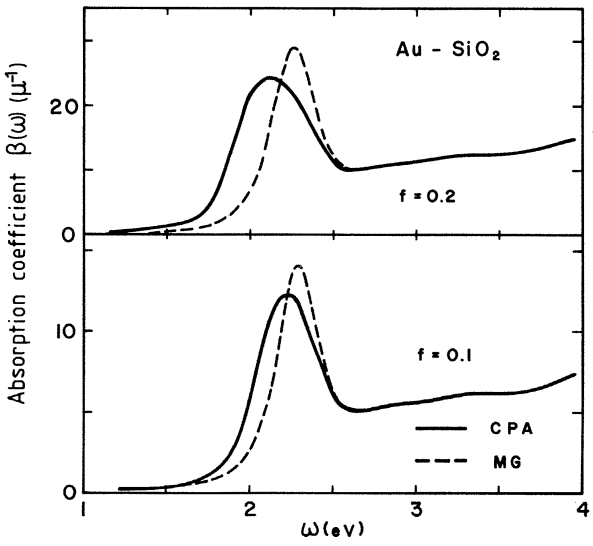

FIG. 14. Absorption spectra for gold particles in SiO_2 at two filling fractions. Solid lines, CPA; dashed lines, MG approximation.

cluded in the theory. Compared to the MG results, however, the CPA gives a red shift of about 0.1—0.25 eV of the absorption peak and is therefore in better overall agreement with the data.

The Drude region in the case of silver is relatively large ($\omega \lesssim 4$ eV), i.e., interband transitions have only a minor influence on the absorption spectra of small particles in the visible. In Fig. 14 calculated absorption spectra are shown for gold particles in SiO_2 ($\epsilon_1 = 2.2$) at filling fractions $f = 10\%$ and 20%. Here the onset of interband transitions occurs at about 2.6 eV. Above this energy, the MG and CPA absorption coefficients coincide, i.e., the disorder is seen to have very little effect. The resonance below this threshold, however, is red shifted and broadened. These kinds of effects have been observed, for example, by Doremus,[23] who studied the absorption spectra of gold particles in glass. Compared to the MG calculation, the measured peaks were found to be broader and located at slightly lower frequencies. Qualitatively similar behavior was also observed for gold particles immersed in other media.[24–28]

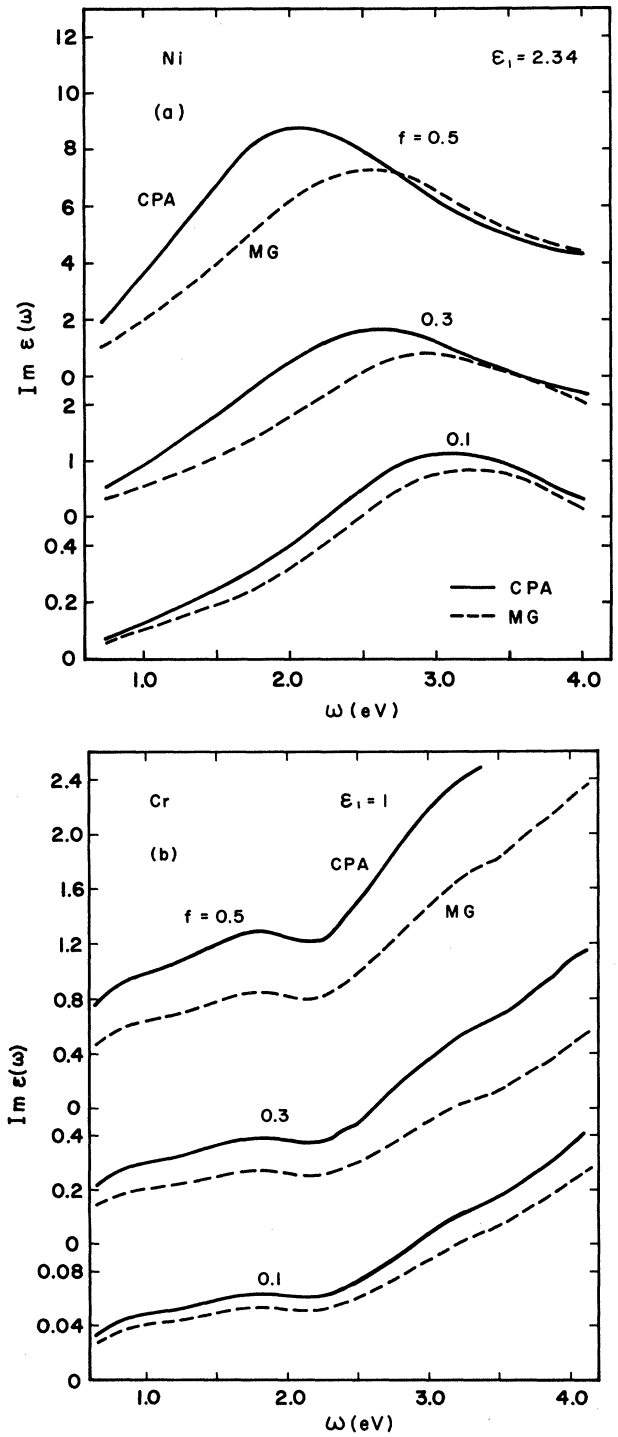

FIG. 15. Imaginary parts of dielectric function for (a) Ni particles in KBr and (b) Cr particles in vacuum for various filling fractions f. Solid lines, CPA; dashed lines, MG approximation.

Although the free-electron region in the case of gold is quite small, the spectra still show the characteristic resonances induced by the finite particle size. A rather different behavior is found in transition metals whose dielectric properties are entirely dominated by interband transitions. To illustrate the influence of randomness on the absorption spectra of these kinds of inhomogeneous systems, we show in Fig. 15 the absorption coefficient for Ni and Cr particles at several filling fractions. The bulk dielectric functions[29] of Ni and Cr are used and the Ni particles are immersed in KBr ($\epsilon_1 = 2.34$), whereas the Cr particles are surrounded by vacuum. Instead of the resonances which are characteristic of Drude particles, a broad absorption spectrum is observed in both cases. The disorder among particles as calculated within the CPA is seen to enhance the absorption coefficient which might also be viewed as an overall red shift of the entire spectrum. Transmittance spectra of chromium particles in air show a strong increase of the transmittance towards long wavelength.[30] The Maxwell-Garnet formula reproduces this increase qualitatively; the onset occurs, however, at too-high energies. The enhancement of $\beta(\omega)$ shown in Fig. 15(b) makes the system less transparent at lower energies, i.e., it shifts the onset of the rise of transmittance to longer wavelength. Thus the CPA treatment of the disorder improves the agreement between calculated and measured spectra.

IV. SUMMARY

We have presented a theoretical treatment of the influence of positional randomness on the optical properties of small metallic particles embedded in a dielectric host. Traditionally, this kind of inhomogeneous system has been analyzed using the Maxwell-Garnett model which is based on the Clausius-Mossotti relation and therefore neglects the contributions to the local electric field arising from the noncubic structure of the composite system. Using the coherent-potential approximation, we have shown that these additional fields lead to an appreciable red shift and broadening of the absorption lines. The central quantity in our theory is the self-consistently determined effective single-particle polarizability in analogy to the effective single-site t matrix in the alloy case. In the Maxwell-Garnett model, this effective polarizability is simply replaced by the true single-particle polarizability multiplied by the particle concentration; i.e., the MG

theory is equivalent to the average—t-matrix approximation.

It should be emphasized that our theory applies to a particular type of composite systems, namely, those of cermet topology in which one constituent is completely surrounded by the other. Thus our treatment should not be confused with the so-called "effective-medium theory"[31] which can also be regarded as a CPA-type theory but which applies to composites consisting of topologically equivalent constituents (i.e., both components must be treated on the same geometrical footing since none can be considered as a host into which the other is embedded). The distinction between these topologies is quite important since they can give rise to strikingly different optical properties.

ACKNOWLEDGMENTS

One of the authors (A.L.) would like to thank the group at the Instituto de Fisica in San Luis Potosí for its hospitality. This work was supported in part by the Organization of American States, and by the German-Mexican Agreement on Scientific and Technological Exchange.

[1] *Electrical Transport and Optical Properties of Inhomogeneous Media,* proceedings of the first Conference on the Electrical Transport and Optical Properties of Inhomogeneous Media, edited by J. C. Garland and D. B. Tanner (AIP, New York, 1978).

[2] A. J. Sievers, in *Solar Energy Conversion,* edited by B. O. Seraphin (Springer, Berlin, 1979), p. 57.

[3] B. O. Seraphin, in *Solar Energy Conversion,* edited by B. O. Seraphin (Springer, Berlin, 1979), p. 5.

[4] B. N. J. Persson and A. Liebsch, Solid State Commun. 44, 1637 (1982).

[5] A. Liebsch and B. N. J. Persson, J. Phys. C 16, 5375 (1983).

[6] P. Soven, Phys. Rev. 156, 809 (1967).

[7] J. C. Maxwell-Garnett, Philos. Trans. R. Soc. London 203, 385 (1904); 205, 237 (1906).

[8] D. J. Bergman, Phys. Rev. Lett. 44, 1285 (1980); Phys. Rev. B 23, 3058 (1981).

[9] G. W. Milton, Appl. Phys. Lett. 37, 300 (1980); Phys. Rev. Lett. 46, 542 (1981).

[10] G. A. Niklasson and C. G. Granqvist, Sol. Energy Mater. 5, 173 (1981).

[11] W. Lamb, D. M. Wood, and N. W. Ashcroft, Phys. Rev. B 21, 2248 (1980).

[12] J. D. Jackson, *Classical Electrodynamics* (Wiley, New York, 1962), Chap. 4.

[13] See, for example, N. W. Ashcroft and N. D. Mermin, *Solid State Physics* (Holt, Rinehart, and Winston, New York, 1976), p. 542.

[14] H. Shiba, Prog. Theor. Phys. 46, 77 (1971).

[15] M. H. Cohen and F. Keffer, Phys. Rev. 99, 1128 (1955).

[16] R. Brako, J. Phys. C 12, 1139 (1979).

[17] D. M. Wood (private communication).

[18] W. T. Doyle, J. Appl. Phys. 49, 795 (1978).

[19] B. N. J. Persson and A. Liebsch, Phys. Rev. B 28, 4247 (1983).

[20] T. Yamaguchi, S. Yoshida, and A. Kinbara, Thin Solid Films 21, 173 (1974).

[21] U. Kreibig, A. Althoff, and H. Pressmann, Surf. Sci. 106, 308 (1981).

[22] P. B. Johnson and R. W. Christy, Phys. Rev. B 6, 4370 (1972).

[23] R. H. Doremus, J. Chem. Phys. 40, 2389 (1964); J. Appl. Phys. 37, 2775 (1966).

[24] J. C. C. Fan and P. M. Zavracky, Appl. Phys. Lett. 29, 478 (1976).

[25] J. I. Gittleman, B. Abeles, P. Zanzucchi, and Y. Arie, Thin Solid Films 45, 9 (1978).

[26] P. H. Lissberger and R. G. Nelson, Thin Solid Films 21, 159 (1974).

[27] D. R. McKenzie and R. C. McPhedran, in *Electrical Transport and Optical Properties of Inhomogeneous Media,* Ref. 1, p. 283.

[28] R. W. Cohen, G. D. Cody, M. D. Coutts, and B. Abeles, Phys. Rev. B 8, 3689 (1973).

[29] P. B. Johnson and R. W. Christy, Phys. Rev. B 9, 5052 (1974).

[30] C. G. Granqvist and G. A. Niklasson, J. Appl. Phys. 49, 3512 (1978).

[31] D. A. G. Bruggeman, Ann. Phys. (Leipzig) 24, 636 (1935); see also Ref. 1.